Journal of Biomolecular NMR (2005) 33: 243–259
DOI 10.1007/s10858-005-3868-4

Article

Extended flip-back schemes for sensitivity enhancement in multidimensional HSQC-type out-and-back experiments

Tammo Diercks*, Mark Daniels & Robert Kaptein
Department of NMR Spectroscopy, Bijvoet Center for Biomolecular Research, Utrecht University, 3584 CH, Utrecht, The Netherlands

Received 8 August 2005; Accepted 26 September 2005

Key words: extended flip-back, fast pulsing regime, magnetisation recovery, orthogonal polarisation separation, resolution enhancement, sensitivity enhancement

Abstract

In many NMR experiments, only polarisation of a limited sub-set of all protons is converted into observable coherence. As recently shown by the ''longitudinal'' TROSY implementation (Pervushin et al. (2002) *J. Am. Chem. Soc.*, **124**, 12898–12902) and SOFAST-HMQC (Schanda and Brutscher (2005) *J. Am. Chem. Soc.*, **127**, 8014–8015), recovery of unused polarisation can be used indirectly and unspecifically to cool the proton lattice and, thus, accelerate re-equilibration for the selected proton subset. Here we illustrate transfer of this principle to HSQC-based multi-dimensional out-and-back experiments that exploit only polarisation of ^{15}N-bound protons. The presented modifications to the pulse sequences can be implemented broadly and easily, extending standard flip-back of water polarisation to a much larger pool of protons that may comprise all non-^{15}N-bound protons. The underlying orthogonal separation of H^N polarisation (selected by the main transfer path) from unused H^u polarisation (flipped-back on the recovery path) is thereby achieved through positive or negative selection by J-coupling, or using band-selective pulses. In practice, H^u polarisation recovery degrades mostly through cumulative pulse imperfections and transverse relaxation; we present, however, strategies to substantially minimise such losses particularly during interim proton decoupling. Depending on the protein's relaxation properties and the extended flip-back scheme employed, we recovered up to 60% H^u equilibrium polarisation. The concomitant cooling of the proton lattice afforded substantial gains of more than 40%, relative to the water-only flip-back version, in the *fast pulsing regime* with re-equilibration delays τ much shorter than optimal ($\tau_{opt} = 1.25 \cdot T_1(H^N)$). These would be typically employed if resolution requirements dominate the total measurement time. Contrarily, if sensitivity is limiting and optimal interscan delays τ_{opt} can be set (*optimal pulsing regime*), the best of the presented flip-back schemes may still afford up to ca. 10% absolute sensitivity enhancement.

Abbreviations: bsfb – band-selective flip-back; cpd – continuous pulsing decoupling; efb – extended flip-back; H^u – unselected proton magnetisation; H^Cfb – H^Cflip-back; ufb – universal flip-back; wfb – water flip-back

Introduction

Many NMR experiments exploit only the polarisation of a selected proton subset on their main coherence transfer path to generate the desired spectrum. All other proton polarisation then remains unused, not being converted into observable coherence. Both pools of proton polarisation are, however, intrinsically coupled via extensive dipolar interactions, enabling

*To whom correspondence should be addressed. Email: tammo@nmr.chem.uu.nl

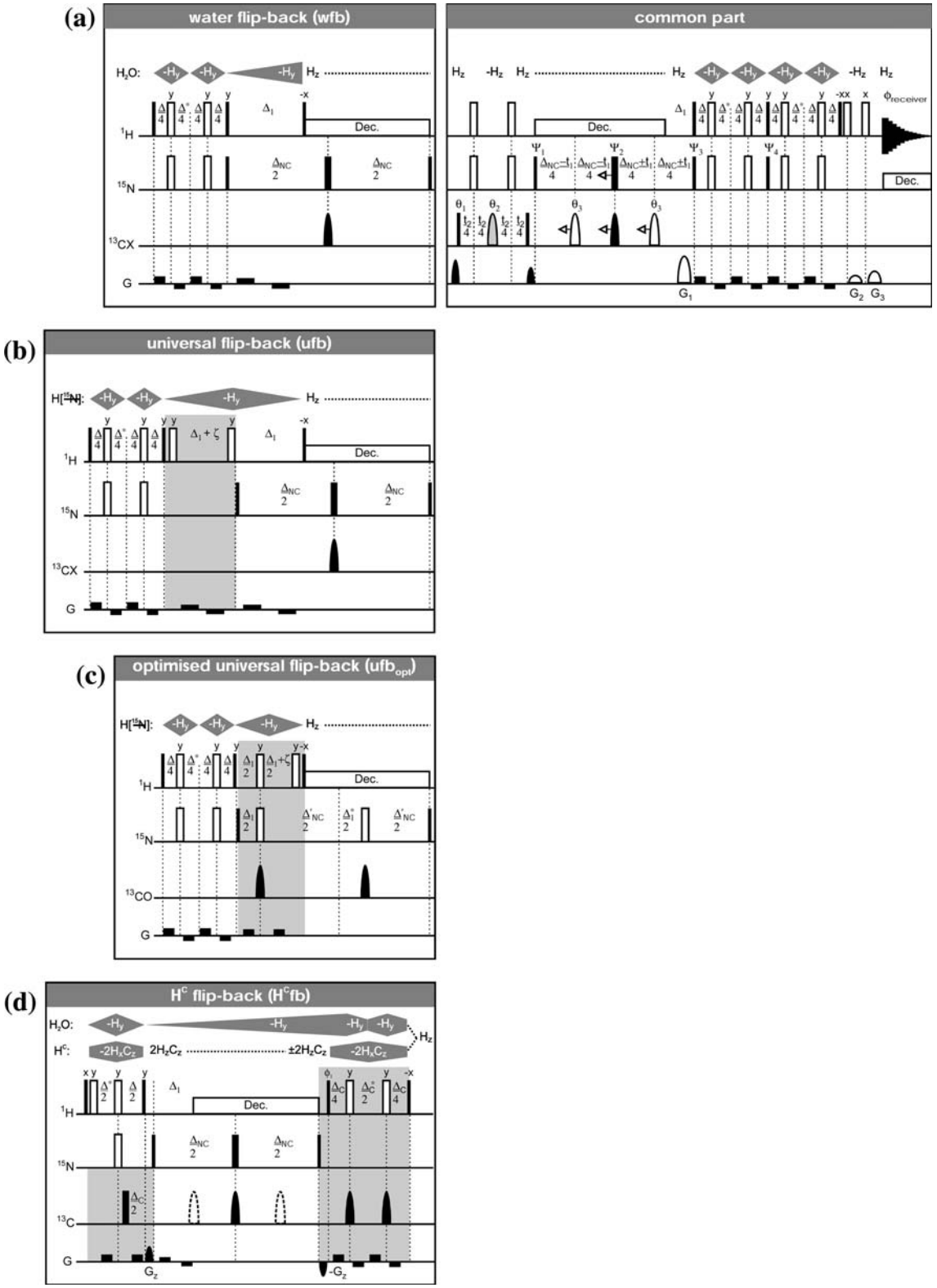
(a)
water flip-back (wfb)
common part
(b)
universal flip-back (ufb)
(c)
optimised universal flip-back (ufb$_{opt}$)
(d)
H^C flip-back (H^{C}fb)

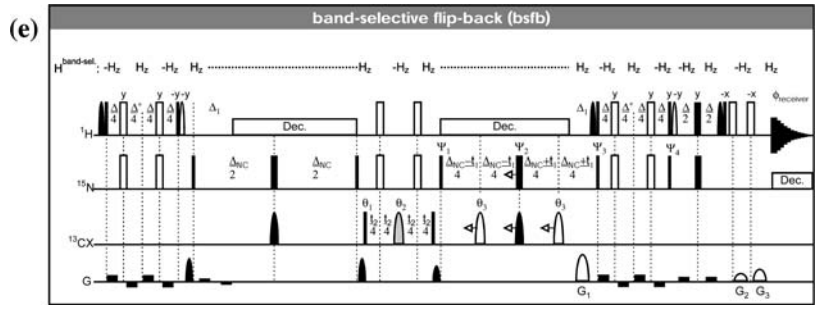

Figure 1. Extended flip-back (efb) modifications of the basic 3D HNCX experiment (CX = CO or CA), with the corresponding H^u polarisation recovery path indicated above. Both the conventional water flip-back version (*wfb*, (a)) and all efb schemes separating recoverable H^u from observed H^N magnetisations by means of J coupling evolution ((b)–(d)) share a common part that includes the t_2 time on ^{13}CX and the subsequent $CX \rightarrow N \rightarrow H^N$ back-transfer. Both the universal flip-back (ufb, (b)) and the optimised ufb scheme that is only applicable for CX = CO (ufb_{opt}, (c)) refocus all non-^{15}N-bound H^u coherence for flip-back by passively exploiting the $^1J_{HN}$ coupling. Alternatively, ^{13}C-bound H^C magnetisation (and water) can be flipped back by actively exploiting the $^1J_{CH}$ coupling (H^Cfb, (d). The band-selective flip-back scheme (bsfb, (e)) employs band-selective 90° pulses throughout for continuous flip-back of H^{bsfb} within the selected frequency range. Indicated narrow and broad square pulses have 90° and 180° flip angle, respectively. Open broad square pulses (on ^1H and ^{15}N) are 180° constant-amplitude BIPs (Smith et al., 2001); for ^1H, we employed the "50-20-720" BIP compensating for $\pm 50\% \cdot B_{rf}$ offset and $\pm 20\% \cdot B_{rf}$ field inhomogeneity with a duration equivalent to a 720° square pulse, and for ^{15}N the "75-15-540" BIP compensating for $\pm 75\% \cdot B_{rf}$ offset and $\pm 15\% \cdot B_{rf}$ field inhomogeneity with a duration equivalent to a 540° square pulse. In the bsfb scheme, band-selective ^1H 90° EBurp2 flip-back pulses (Geen and Freeman, 1991) of ca. $1.5\mu s \cdot \omega_H[MHz]$ duration (e.g., 1 ms at 700 MHz) and shifted to 2 ppm were used without (filled) or with time-reversal (open shapes). CPMG-derived XY16 decoupling (using default 180° square pulses without power reduction and ca. 200–300 μs echo delays) is suggested for broadband proton decoupling with maximal preservation of recovered H^u polarisation. Open selective 180° decoupling pulses on CO or CA have Gauss or Q3 (Emsley and Bodenhausen, 1992) shape, respectively; the ^{13}C decoupling pulse in t_2 (filled grey) thereby is cosine-modulated for compensation of Bloch-Siegert shifts (Sattler et al., 1999). Filled selective 180° pulses on ^{13}C (Gauss for CX = CO, Q3 for CX = CA) must invert CX only, except in the H^Cfb scheme where broadband inversion (e.g., by BIP) of all ^1H-bound ^{13}C is required for CX = CA; in this case, the dashed selective CO decoupling pulses (e.g., Gauss) must likewise be applied. Default pulse phase is x unless stated otherwise, with the following phase cycles: $\phi_1 = y$ (CX = CO) or $-y$ (CX = CA); $\theta_1 = \theta_3 = x, -x$; $\theta_2 = x, x, y, y$; $\psi_1 = x, x, -x, -x$; $\psi_2 = x$ (4×), y (4×); $\psi_3 = x \times 8, -x \times 8$; $\psi_4 = y \times 8, -y \times 8$; $\phi_{receiver} = (x, -x, -x, x), (-x, x, x, -x) \times 2, (x, -x, -x, x)$. Delays: $\Delta \leq (2^1J_{HN})^{-1}$, $\Delta_1 = (2^1J_{HN})^{-1}, \Delta_{NC} \leq (2^1J_{NCX})^{-1}, \Delta_{NC'} = \Delta_{NC} - \Delta_1, \Delta_C \leq \langle 2^1J_{HC} \rangle^{-1}, \zeta = p_{90°}(^{15}N) + (4/\pi) \cdot p_{90°}(^1H)$, $p_{90°} = 90°$ pulse length; delays marked with a superscript asterisk are extended by $(4/\pi) \cdot p_{90°}(^1H)$ for optimal rephasing within BIP pairs. Open gradients $G_{1\text{-}3}$ of equal duration select ^{15}N coherence in t_1 by setting $G_3 - G_2 = (\gamma_H/\gamma_N) \cdot G_1 = 0.101 \cdot G_1$ in the antiecho path. For echo detection in F1(^{15}N), gradient G_1 is inverted along with phase ψ_4 for sensitivity enhancement. For complex quadrature detection in F2(^{13}CX), phase θ_1 is alternated between x and y for successive t_2 increments. Weak filled gradient pairs are used throughout to suppress radiation damping (Sklenar, 1995). The presented efb-enhanced HNCX pulse sequences (BRUKER format) can be downloaded at http://www.nmr.chem.uu.nl/~tammo.

cross-relaxation that eventually establishes a common spin temperature in a phenomenon referred to as "spin diffusion" (Abragam, 1961). The spin temperature of the ambient proton lattice thus importantly affects re-equilibration of the signal-generating proton subset, where T_1 relaxation progresses substantially faster under selective (with all except the selected proton spins near thermal equilibrium) than under unselective conditions (with uniformly depleted initial magnetisation for all protons). Experimentally cooling the spin temperature of the proton lattice can thus afford sizeable sensitivity gains through cross-relaxation accelerated polarisation recovery, as recently demonstrated for TROSY-type experiments (Pervushin et al., 2002) and 2D HMQC (Schanda and Brutscher, 2005).

Here, we present analogous modifications to multidimensional HSQC-type out-and-back experiments where the magnetisation path starts and ends on the same selected proton and, in the absence of indirect proton evolution times, all unselected proton polarisation could in priciple remain unperturbed. This important class of experiments comprises, e.g., triple resonance HNCO, HNCA, HNCACO, HNCOCA and HNCACB (Sattler et al., 1999) that all exploit exclusively H^N polarisation. Conventional implementations, however, so far unheedingly waste the vast pool of unused H^u proton polarisation, being designed only to restore water polarisation. The presented modifications extend water flip-back to comprise polarisation of the larger part of, or all unselected protons, separating it from

H^N polarisation by means of scalar coupling evolution or band-selective pulses. Absent in HMQC and TROSY-type experiments, interim proton decoupling thereby requires adjustment to maximally preserve flipped-back H^u polarisation. With the spin temperature of the ambient proton lattice thus cooled substantially, we illustrate achievable enhancements in the signal-to-noise ratio from accelerated recovery of H^N polarisation.

Extended flip-back schemes

Common to the family of out-and-back triple resonance experiments investigated here is the HNCX building block with CX = CA or CO. We therefore restrict the discussion of modifications for *e*xtended *f*lip-*b*ack (efb) of *u*nused H^u polarisation to this basic three-dimensional experiment. Inserting further heteronuclear transfer steps into the t_2 evolution time on CX to compose HNCXCY derivatives (where CY = CO, CA or CB) is then straightforward and compatible with the efb afforded by the presented schemes. These can be classified in two categories, based on whether scalar *J*-coupling evolution or band-selective pulses are employed for the required orthogonal separation between selected H^N and recoverable H^u magnetisations. The first category may again be sub-divided into passive separation by the same $^1J_{HN}$ coupling also exploited in the main transfer path to achieve *u*niversal *f*lip-*b*ack (ufb) of *all* unused non-^{15}N-bound protons, or active separation by the vacant $^1J_{H_C}$ coupling for ^{13}C-bound H^C proton *f*lip-*b*ack (H^Cfb) only. The use of selective pulses likewise achieves non-universal, *b*and-*s*elective *f*lip-*b*ack (bsfb).

Figure 1 illustrates efb modifications of the basic sensitivity-enhanced HNCX experiment (Kay et al., 1994) along with their corresponding H^u polarisation recovery paths. Except for the bsfb version, modifications are restricted to the initial $H^N \longrightarrow N \longrightarrow CX$ out-transfer part. The common part, including t_2 shift evolution on CX and subsequent $CX \longrightarrow N \longrightarrow H^N$ back-transfer with sensitivity enhancement, intrinsically achieves flip-back of present polarisation with proper phase settings. Conventionally, the pulse sequence only achieves on-resonant *w*ater *f*lip-*b*ack (wfb, Figure 1a) as it fails to refocus H^u chemical shift evolution for offsets $\neq 0$ during the $^1J_{HN}$ rephasing period Δ_1 in the $H^N \longrightarrow N$ reINEPT. Universal refocussing for all non-^{15}N-bound protons can be achieved with the ufb scheme (Figure 1b), where a 180°(^{1}H) rephasing pulse is applied simultaneously with the first 90°(^{15}N) excitation pulse after inserting a compensating H^u shift evolution delay Δ_1'. This central 180°(^{1}H) pulse thereby also decouples H^u coherence from any J_{HX} coupling evolution during Δ_1' and Δ_1. During the inserted delay Δ_1' (ca. 4–5 ms), the main coherence transfer path adopts $2H_zN_z$ spin order that may then, however, accrue noticeable losses from T_1 relaxation and H^N-water exchange. An optimised ufb_{opt} scheme (Figure 1c) therefore concatenates the refocussing of H^u coherence with the rephasing of $2N_yH_z$ antiphase coherence during Δ_1 in the $H^N \longrightarrow N$ reINEPT. In order to evolve the $^1J_{HN}$ coupling, and the J_{NCX} coupling for the entire length of the delay Δ_{NC}, 180° pulses on ^{15}N and CX must be applied simultaneously with the inserted 180°(^{1}H) pulse. This, however, also activates any J_{HCX} coupling for CX-bound H^u coherence during Δ_1, obviating its recovery. The ufb_{opt} scheme may therefore only be used for negligible J_{HCX} coupling, i.e. for CX = CO. Contrarily, the H^Cfb scheme (Figure 1d) constructively exploits the substantial $^1J_{HC}$ coupling to prepare $2H_zC_z$ and $2H_zN_z$ spin order concomitantly in the intial INEPT by suitably inserting a 180°(^{13}C) pulse. ^{13}C-bound H^u polarisation is thus stored as $2H_zC_z$ during the subsequent N⟶CX transfer step, and then converted back to pure H_z^u magnetisation by a second H,C-INEPT module inserted while the main transfer path adopts proton-decoupled, and largely T_1-insensitive, $2N_zCX_z$ spin order. The central CX inversion pulse in the N ⟶CX transfer step, required for J_{NCX} coupling evolution, must now affect the stored $2N_zC_z$ order uniformly for all protonated ^{13}C. Uniform non-perturbation of $2N_zC_z$ can be achieved for CX = CO only, using a CO-selective inversion pulse. In contrast, frequency discrimination between CX = CA and all other protonated ^{13}C is impossible, requiring their uniform inversion. The resulting inversion of stored $2N_zC_z$ order must then be compensated by inverting ϕ_1 in the H,C-INEPT reconversion module. Water magnetisation, although not ^{13}C-bound, is still flipped-back by the H^Cfb scheme if kept on-resonant, but only at the end of the inserted second H,C-INEPT

module. In contrast to all other schemes, water magnetisation may consequently degrade from faster T_2 relaxation during the first $N \longrightarrow CX$ transfer step; furthermore, radiation damping should be suppressed by applying the indicated G_z gradient echo. Finally, the bsfb modification (Figure 1e) exploits the frequency difference between H^N and the major part of (aliphatic) H^u resonances by continuously employing band-selective 90° pulses on the latter to immediately compensate the effect of any unselective 90° proton pulse. For flip-back, the water frequency must be covered by the band-selective pulses as well.

While the presented efb schemes afford magnetisation flip-back for different sets of H^u protons, they also differ in their susceptibility to T_2 relaxation as a main attrition factor for polarisation recovery. The polarisation recovery paths indicated in Figure 1 reveal that H^u magnetisation spends a total duration of $3\Delta + \Delta_C$ for H^Cfb, 4Δ for ufb_{opt} and 5Δ for ufb in the transverse plane, accumulating increasing T_2 relaxation losses while some dephasing from homonuclear $^nJ_{HH}$ proton coupling may be neglected. Consequently, the ufb_{opt} scheme is relaxation-optimised with respect to simple ufb for both the H^N-derived coherence transfer (see above) and the H^u polarisation recovery paths; it may, however, only be used for CX = CO. The H^C fb scheme slightly shortens the total H^u coherence time by another $\Delta - \Delta_c$, yet at the expense of restricting polarisation recovery to ^{13}C-bound protons. The non-uniform $^1J_{CH}$ couplings here further compromise complete preparation of temporarily stored $2H_zC_z$ order that also decays somewhat faster than the H_z^u polarisation stored in all other cases. The H^Cfb scheme should therefore remain inferior to ufb_{opt} and be considered only when the latter cannot be employed, i.e. for CX = CA. In contrast to the efb schemes separating H^N and H^u magnetisation by J coupling evolution, minimal T_2 relaxation losses (i.e., practically only during pulses) accrue for the recovered H^u polarisation in the bsfb modification. Polarisation recovery here should therefore be substantially increased, while being restricted to those H^u proton frequencies covered by the band-selective pulses. In case of overlap between H^N and H^u (including H_2O) frequencies, flip-back has to be restricted even more severely.

Cumulative imperfections in the numerous ^{1}H pulses (from miscalibration, B_{rf} inhomogeneity or offset-dependence) may also importantly degrade H^u polarisation recovery. In contrast to T_2 relaxation, however, this attrition factor may be minimised by appropriate experimental means (e.g., Hallenga and Lippens, 1995; Zweckstetter and Holak, 1999). As shown in Figure 1, we thus substituted the more error-prone 180° pulses by broadband inversion pulses (BIP) with optimised tolerance to B_{rf} inhomogeneity and miscalibration (Smith et al., 2001); substituting the less error-prone square 90° pulses by more robust alternatives like, e.g., BeBop (Skinner et al., 2004) might be envisaged additionally. When applied to coherence on either the polarisation recovery or main transfer path, BIPs must be inserted pairwise for mutual compensation of phase errors. Consequently, every single 180° square pulse on ^{1}H and, simultaneously, ^{15}N was replaced by BIP pairs, except during the second transfer step of the sensitivity-enhanced reINEPT in the bsfb scheme. The need to mutually compensate the Bloch–Siegert shifts induced by both inserted band-selective 90° flip-back pulses here required us to retain the single square 180° pulse. Substituting square 180° pulses for BIP (pairs) has relevance beyond the methods detailed here, reducing losses on both the H^upolarisation recovery and H^N coherence transfer path. Ca. 2.5% intensity gains per pairwise BIP implementation were thus obtained even with the wfb scheme, while the tolerance towards pulse miscalibration was dramatically enhanced, yielding identical intensities even with a BIP power missetting by ± 2 dB. We therefore strongly recommend to implement BIPs in NMR pulse sequences more generally.

Mutual compensation of some imperfections in successive pulses can also be achieved through proper choice of relative phases, always within the constraints imposed by the main coherence transfer path. Most importantly, and generally proposed for spin echoes (Meiboom and Gill, 1958), any 180° pulse must therefore be applied with a phase perpendicular to the preceding 90° excitation pulse. For the same reasons, and likewise considered in the schemes depicted in Figure 1, we found that the first and last band-selective flip-back pulses in the final sensitivity-enhanced $^{15}N \rightarrow ^1$H back-transfer of the bsfb scheme must be applied with identical phases.

Optimised proton decoupling schemes

A distinct component of most HSQC-based triple resonance experiments is interim proton decoupling to suppress formation of anti-phase $2H_zX_y$ coherence, which generally relaxes faster than its in-phase counterpart due to dipolar proton–proton interactions. In the out-and-back HNCX experiments investigated here, proton decoupling is required during the long N↔CX transfer steps where temporary anti-phase $2H_zN_y$ coherence could additionally decay by H^N/water exchange. Interim proton decoupling, however, inadvertently interferes with the desired H^u polarisation recovery except in perfectly band-selective homonuclear decoupling of amide protons only. Yet, this is inachievable in practice and moreover introduces a frequency-selection during ^1H decoupling that contravenes the frequency-independent H^u magnetisation flip-back afforded by all efb schemes except bsfb, where it might be implemented advantageously. We therefore only considered broad-band proton decoupling schemes supporting *universal* H^u flip-back as well. Obviously, when using standard *c*ontinuous *p*ulsing *d*ecoupling (cpd) sequences, their duration must be matched to full supercycles to eventually bring recovered H^u magnetisation back to its initial *z*-alignment. Still, the proton trajectory during any cpd sequence spends much of the time in the transverse plane, accumulating substantial T_2 relaxation losses. Decoupling by means of a single 180° proton inversion pulse would eliminate this source of losses for the recovered H^u polarisation (trading it for rather insignificant T_1 relaxation losses), yet fail to efficiently suppress $2H_zN_y$ anti-phase formation. The obvious compromise is then discontinuous "windowed" CPMG-type decoupling, using a repetition of proton inversion pulses at reasonably short intervals. Imperfections and the limited bandwidth of these pulses must, however, be compensated by appropriate phase cycling (Gullion et al., 1990) to ensure sufficient, broadband H^N decoupling as well as preservation of recovered H^u polarisation. Such phase-cycled derivatives of the classic CPMG sequence perform excellently even for broadband isotropic Hartmann–Hahn mixing (Furrer et al., 2004), corroborating their equal suitability for the less demanding task of broadband H^N decoupling. The echo delay δ_{CPMG} should then be chosen long enough to maintain a low duty cycle and reduce sample heating, but short enough to prevent substantial $2H_zN_y$ anti-phase formation and reduce T_2 relaxation losses for interim stray H^u coherence produced by imperfect inversion pulses and partially recovered through the phase cycling scheme. For instance, choosing $\delta_{CPMG} = 200$–550 μs, i.e. $(4\text{–}10\%)\times(2^1J_{HN})^{-1}$, would still limit $2H_zN_y$ anti-phase formation during each interval to negligibly small 0.3–3%. The required decoupling duration can then be realised much easier than with cpd sequences by simply adjusting the echo delay δ_{CPMG} and, possibly, the number of full supercycles.

Accelerated H^N relaxation and sensitivity enhancement

As previously exploited in LTROSY (Pervushin et al., 2002) and SOFAST-HMQC (Schanda and Brutscher, 2005), the substantial H^u polarisation recovered by the presented efb schemes can be used straightaway to indirectly replenish depleted H^N polarisation during the subsequent interscan delay τ (defined as the total delay between last and first proton pulse in consecutive scans). This constructive effect of dipolar $H^u \rightarrow H^N$ cross-relaxation accelerates recovery of H^N polarisation and entails a reduction in net $T_1(H^N)$ relaxation times at the expense of $T_1(H^u)$, which in turn results in increased signal intensities if H^N relaxation remains incomplete during short $\tau \ll 3 \cdot T_1(H^N)$. Consequently, the sensitivity enhancement afforded by H^u polarisation recovery should increase with the pulsing rate, i.e. with decreasing τ. We may obtain some insight into this dependence by starting from the well-known expression for the signal-to-noise ratio, SN (Ernst et al., 1987), with $R_1(H^N) = 1/T_1(H^N)$:

$$SN \propto \left[1 - \exp\left(-\tau \cdot R_1\left(H^N\right)\right)\right] \cdot \sqrt{n_s} \qquad (1)$$

The balance between H^N relaxation during τ and both signal and noise accumulation by the n_s scans produces a maximum SN_{max} for a distinct optimal interscan delay τ_{opt} (Pervushin et al., 2002):

$$\tau_{opt} \approx 1.25 \cdot T_1(H^N) \qquad (2)$$

Using this expression and the substitution $n_s \approx T_{total}/\tau$ (where T_{total} is the total measure-

ment time per increment), Equation (1) transforms into:

$$\mathrm{SN}(\tau) \propto \left[1 - \exp(-1.25 \cdot \tau/\tau_{\mathrm{opt}})\right] \cdot \sqrt{\frac{T_{\mathrm{total}}}{\tau}} \tag{3}$$

The τ-dependent sensitivity enhancement afforded by accelerated H^N re-equilibration then corresponds to the ratio of SN values (or, simply, signal intensities) measured for experiments of *equal* duration T_{total} employing different H^u polarisation recovery schemes:

$$\left[\frac{\mathrm{SN}^{\mathrm{f}}}{\mathrm{SN}^{0}}\right](\tau) = \frac{c^{\mathrm{f}}}{c^{0}} \cdot \frac{\left[1 - \exp\left(-1.25 \cdot \tau/\tau^{\mathrm{f}}_{\mathrm{opt}}\right)\right]}{\left[1 - \exp\left(-1.25 \cdot \tau/\tau^{0}_{\mathrm{opt}}\right)\right]} \tag{4}$$

Here and in the following, superscripts 0 (denoting the conventional reference wfb scheme) and f (designating one of the presented efb schemes) indicate values that generally depend on the H^u flip-back factor $f \leq 1$ (see below) and/or relative H^N intensity scaling factor $c^f \leq 1$ pertaining to a given flip-back scheme. Factor c^f thus comprises all additional losses accumulating on the coherence path using a given efb scheme, relative to the reference wfb implementation with a c^0 defined to be 1. While the latter should afford no H^u magnetisation flip-back, an $f^0 > 0$ may nonetheless result from some direct (i.e., concomitant flip-back for H^α resonating near the water frequency) and indirect (i.e. labile protein protons exchanging with the water) H^u polarisation recovery that may become quite substantial for very large proteins (Riek et al., 2002).

Equation (4), plotted in Figure 2, immediately reveals that any sensitivity enhancement from accelerated H^N relaxation vanishes for long $\tau \gg \tau^{\mathrm{f}}_{\mathrm{opt}}$, when relaxation becomes virtually complete. This *slow pulsing regime* allows to measure the relative H^N intensity scaling factor c^f for a chosen efb scheme and constant experiment time T_{total}:

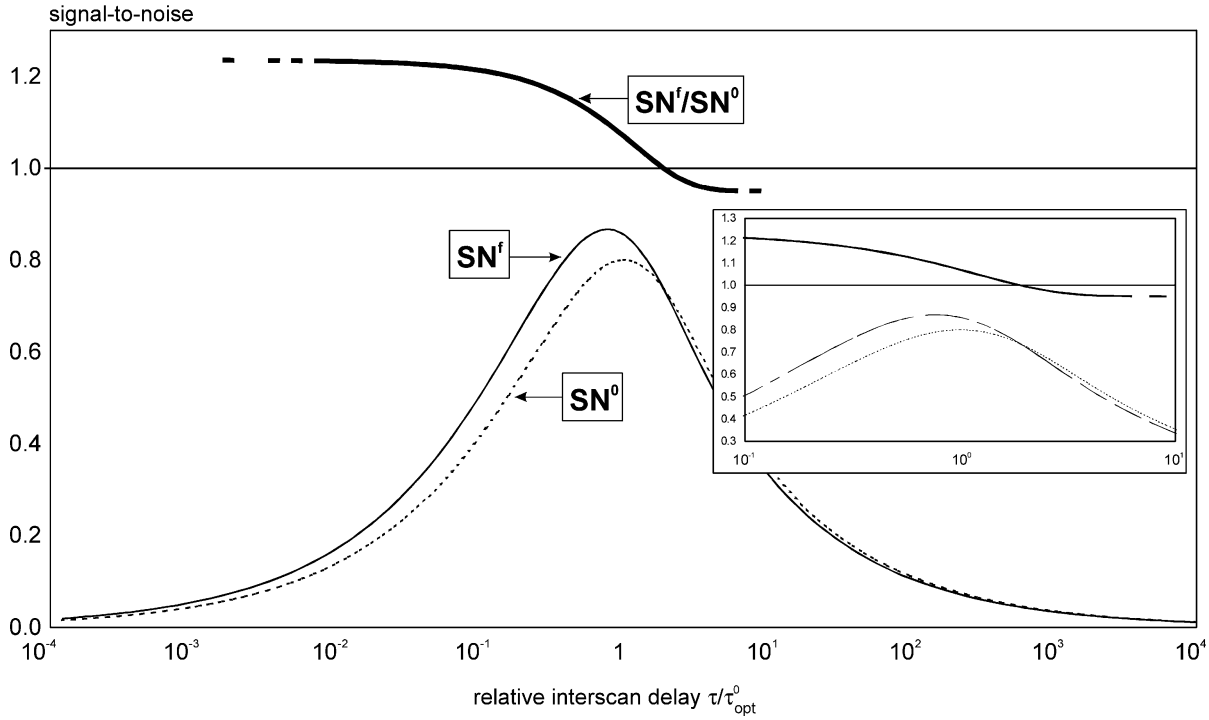

Figure 2. Signal-to-noise ratios without (SN^0) and with efb-accelerated H^N re-equilibration (SN^f), simulated using Equations (3) and (4) on the assumption of constant $R_1(H^N)$ rates with ratio $R_1^f/R_1^0 = 1.3$ (i.e. $\tau^0_{\mathrm{opt}}/\tau^f_{\mathrm{opt}} = 1.3$) and relative scaling factors $c^f/c^0 = 0.95$. The total interscan delay τ is given in units of τ^0_{opt}, for which maximal SN^0 without H^u polarisation recovery is reached. Inserted is a close-up view of the region around τ_{opt} for better comparison with the experimental data shown in Figure 5.

$$\left[\frac{SN^f}{SN^0}\right]_{min}(\tau \gg \tau^f_{opt}) = \frac{c^f}{c^0} \quad (5)$$

Contrarily, maximal *relative* sensitivity enhancement is reached at short $\tau \ll \tau^0_{opt}$ (i.e. *fast pulsing regime*), corresponding to the inverse ratio of the optimal interscan delays pertaining to both flip-back schemes compared:

$$\left[\frac{SN^f}{SN^0}\right]_{max}(\tau \ll \tau^f_{opt}) \leq \frac{c^f}{c^0} \cdot \frac{\tau^0_{opt}}{\tau^f_{opt}} \quad (6)$$

Note, however, that the extent of H^u polarisation recovery underlying the acceleration of H^N relaxation is itself subject to τ-dependent saturation. An equation describing this dependence is derived in the Appendix, or may be deduced from a related equation describing longitudinal interference in repetitive pulse experiments (Ernst et al., 1987; Hiller et al., 2005):

$$\frac{H^u(\tau)}{H^u_0} \equiv f(\tau) = f_0 \cdot \frac{1 - \exp(-\tau \cdot R_1(H^u))}{1 - f_0 \cdot \exp(-\tau \cdot R_1(H^u))} \quad (7)$$

where H^u_0 is the fully re-equilibrated H^u polarisation, $R_1(H^u)$ its longitudinal relaxation rate, and f_0 the intrinsic flip-back factor afforded by a given efb scheme in the absence of saturation, i.e. for $\tau \gg 1/R_1(H^u)$. With the $H^u(\tau)$ polarisation thus vanishing as τ approaches 0, acceleration of H^N relaxation will likewise vanish, and $SN^f(\tau \to 0)$ becomes equal to SN^0. *Relative* sensitivity enhancement will therefore again drop towards its minimum given by Equation (5), after passing through a distinct maximum within the interval $0 < \tau < \tau^f_{opt}$ that may be somewhat smaller than the one given by Equation (6). A more quantitative desciption of the complex relationship between τ-dependent H^u polarisation recovery, f, and generally multi-exponential longitudinal H^N relaxation is, however, beyond the scope of this paper.

Equation (6) nevertheless proves that implementing efb is particularly attractive as a time-saving method if resolution, rather than sensitivity, limits the total measurement time T_{total} for a multi-dimensional experiment: In this resolution-limited regime, only a shortening of τ can further reduce $T_{total} \approx n_s \cdot \tau \cdot n_i$ since the numbers of scans (n_s) and increments (n_i) have both reached their acceptable minima. For a given T_{total}, n_i and, thus, the resolution may then be increased. Alternatively, n_s could be increased to enhance the signal-to-noise ratio for samples limited by sensitivity; one should then choose $\tau = \tau_{opt}$ for maximal SN_{max} (see above). The sensitivity enhancement afforded by H^u polarisation recovery then follows from Equation (3), keeping in mind possible reductions from partial saturation of recovered H^u polarisation (see above):

$$\frac{SN^f_{max}}{SN^0_{max}} = \frac{SN^f(\tau^f_{opt})}{SN^0(\tau^0_{opt})} \leq \frac{c^f}{c^0} \cdot \sqrt{\frac{\tau^0_{opt}}{\tau^f_{opt}}} \quad (8)$$

This maximal *absolute* enhancement is relevant for measurements limited by sensitivity and is reached in the *optimal pulsing regime*, where τ is set to the corresponding τ_{opt} (cf. Equation 2). It is clearly smaller than the maximal *relative* enhancement given by Equation (6) that is relevant for measurements limited by resolution, where uniform τ much shorter than τ_{opt} are employed (*fast pulsing regime*).

Experimental results and discussion

Extent of unused H^u proton polarisation recovery

All efb schemes presented in Figure 1 were experimentally verified on a BRUKER Avance700 spectrometer using several [U−^{15}N,^{13}C] labelled proteins of different size: chymotrypsin inhibitor 2 (CI2, 64 residues) (Ludvigsen et al., 1991), CHD7 (80 residues), hUSP15-DUSP domain (USP, 141 residues) (de Jong et al., submitted) and an hRTFl domain (RTF, 153 residues).

In order to quantify the achievable H^u polarisation recovery, the basic HNCX sequence with efb implementation was modified to record the plain ^{1}H spectrum remaining immediately after the experiment. We thus fixed t_1 and t_2 to zero and appended a standard one-dimensional ^{1}H pulse sequence [90°(H_2O selective) – 90°(^{1}H) – G_0 – (3-9-19) – G_0] with flip-back and suppression of water just prior to acquisition. Here, the global 90° ^{1}H read pulse has the same phase as the receiver and is

preceded by a water-selective 90° flip-back pulse with inverse phase; the composite (3-9-19) rephasing pulse (Sklenar et al., 1993) is surrounded by two identical B_0 field gradients G_0 for water suppression. Note that this modified 1D H[HNCX] experiment inadvertently exhausts all recovered H^u polarisation by conversion into observable coherence, and should no longer contain H^N intensity. For referencing, the complete re-equilibrated ^1H spectrum was obtained after inserting a sufficiently long recovery delay ($\geq 3 \cdot T_1$) just prior to this appended read-out sequence. Due to the inapplicability of the ufb_{opt} scheme if CX = CA, we only illustrate the experimental results for the basic HNCO experiment that allows implementation and direct comparison of all presented efb schemes.

Results for the HNCA-derived experiments were equivalent apart from the expected failure of H^u flip-back using the ufb_{opt} scheme, with negligible H^u polarisation losses from additional R_1 relaxation during the longer interim proton decoupling periods required for evolving the smaller J_{NCA} coupling.

Figure 3 and Table 1 illustrate the substantial H^u proton polarisation recovered at the end of an HNCO experiment employing any of the proposed efb schemes (with pairwise BIP substitution and CPMG-type interim XY16 proton decoupling during the $^{15}N \rightarrow ^{13}CO$ coherence transfer steps). In accordance with the previous reflections, polarisation recovery clearly correlates with the total H^u coherence time spent on the recovery path

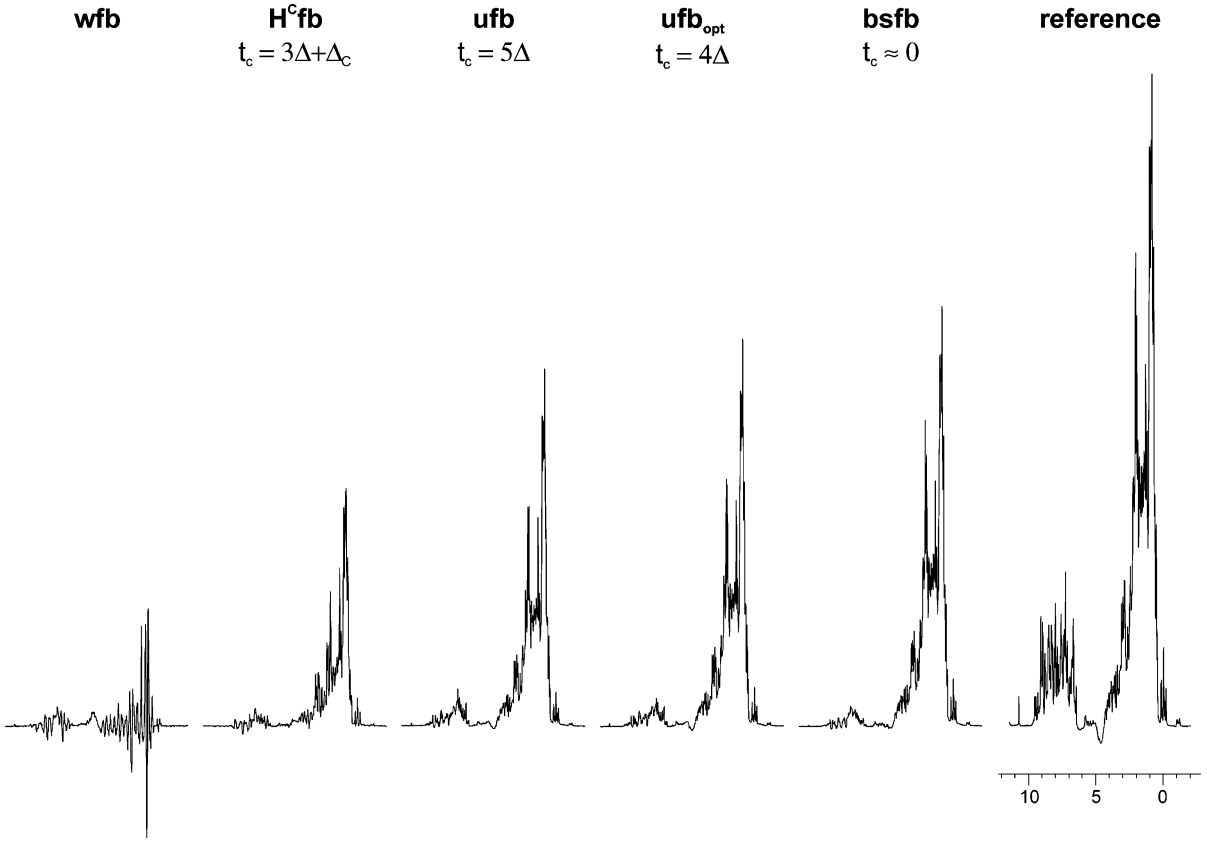

Figure 3. Recovery of unused H^u proton polarisation by the indicated extended flip-back (efb) schemes shown in Figure 1. In contrast to conventional water-only flip-back (wfb), substantial proton (except depleted H^N) polarisation is recovered by any of the proposed efb schemes. Recoveries are largely dominated by T_2 relaxation losses accumulating during the indicated net durations t_c that recovered H^u magnetisation spends in the transverse plane for the given efb scheme ($\Delta \leq (2^1J_{HN})^{-1}, \Delta_C \leq (2^1J_{HC}^{-1})$). All ^1H spectra (at 700 MHz, 298 K) were recorded for CI2 (64 residues) immediately after an HNCO experiment with the indicated flip-back scheme and 2×18.4 ms CPMG-derived XY16 proton decoupling (using 276 μs echo delay and standard 180° square pulses without power switching) during the $^{15}N \rightarrow ^{13}CO$ coherence transfer. The interscan delay was set to 10 s for full re-equilibration; $\Delta = 5$ ms, $\Delta_C = 3.4$ ms. The complete ^1H reference spectrum was recorded similarly, but with another 10 s full recovery delay inserted just prior to the read-out of remaining proton polarisation.

Table 1. H^u polarisation recoveries obtained for various test proteins with the efb schemes shown in Figure 1

	HNCO-bsfb	HNCO-ufb$_{opt}$	HNCO-ufb	HNCO-H^{c}fb
RTF (153 residues)				
$\tau = 10$ s	52%	32%	27%	21%
CHD7 (80 residues)				
$\tau = 10$ s	62%	52%	47%	33%
$\tau = 1$ s	49% (51%)	42% (41%)	36% (36%)	25% (24%)
$\tau = 0.5$ s	37% (40%)	31% (31%)	27% (26%)	20% (17%)
CI2 (64 residues)				
$\tau = 10$ s	63%	56%	50%	30%
$\tau = 10$ s (DIPSI2)[a]	45%	42%	37%	21%
$\tau = 1$ s	48%(51%)	42%(44%)	38% (38%)	24%(21%)
$\tau = 0.5$ s	36% (39%)	32%(33%)	28%(27%)	19%(14%)

Approximate H^u polarisation recoveries were obtained from bulk integration of the remaining ID ^{1}H spectrum acquired immediately after an HNCO experiment employing the indicated efb scheme. Reference is a comparable standard ID ^{1}H spectrum recorded without HNCO prehistory. H^u polarisation recoveries were measured with the indicated total interscan delays τ (including the FID acquisition delay). Full re-equilibration was assumed for $\tau = 10$ s and the corresponding values were equated with the intrinsic flip-back factors *fo*. For shorter $\tau = 1$ and 0.5 s, values in brackets were back-calculated from f_0 using Equation (7) and assuming approximate mono-exponential $T_1(H^u)$ relaxation times of 1050 ms for CI2 and 960 ms for CHD7. Experiments were recorded at 700 MHz, 298 K, using $\Delta \leq (2^1J_{HN})^{-1} = 5$ ms, $\Delta_C \leq (2^1J_{HC})^{-1} = 3.4$ ms, $\Delta_{NC'} \leq (2^1J_{NC'})^{-1} = 23.2$ ms, CPMG-derived XY16 ^{1}H decoupling (except in [a] where DIPSI2 cpd was employed) during 2×18.2 ms with $\delta_{CPMG} = 220\,\mu$s echo delay, pairwise substitution of 180° ^{1}H and ^{15}N pulses by BIP. The bsfb scheme used band-selective EBurp2 90° flip-back pulses of 1 ms duration and centered at 2 ppm.

in the different efb schemes, during which T_2 relaxation acts as the main attrition factor. Thus, ufb and ufb$_{opt}$ (with 5Δ and 4Δ H^u coherence times, respectively; $\Delta \leq (2^1J_{HN})^{-1}$) benefit most from reduced T_2 relaxation of the smaller test proteins, where H^u recovery increased by 2/3 from approximately 30% for the large RTF to ca. 50% for the smaller CHD7 and CI2 proteins when starting with fully re-equilibrated proton polarisation (i.e., interscan delay $\tau = 10$ s). The H^{C}fb recovery scheme, additionally compromised by J_{CH} heterogeneity and T_1 relaxation of the temporarily stored $2C_zH_z$ magnetisation, resulted in relative H recovery losses of 25– 40%. Yet, 40–50% losses accumulated even for the bsfb scheme, where the coherence time spent on the H^u recovery path and ensueing T_2 relaxation losses are apparently eliminated.

Trying to account for these remaining 40–50% H^u polarisation losses from causes other than T_2 relaxation, we first replaced the employed band-selective EBurp2 (Geen and Freeman, 1991) with short unselective square pulses. Losses accrueing during the former could thus be estimated at ca. 5%. Switching off the interim XY16 proton decoupling revealed another, more substantial 20–25% H^u recovery losses at this stage (also see Figure 4). By varying the duration of decoupling, pertaining losses could be attributed approximately one half each to still uncompensated inversion pulse imperfections and to T_1 relaxation degrading the periodically inverted H^u polarisation. The remaining ca. 20% losses in H^u recovery were apparently caused by imperfections in all other proton pulses not yet accounted for. Neglecting attrition from the vastly compensated BIP pulses employed here (Smith et al., 2001), these losses would accrue during the one remaining 180° and five 90° square ^{1}H pulses of the HNCO-bsfb sequence (see Figure 1e), implying realistic ca. 3.5% loss per 90° rotation. Verifying the improvements afforded by the implemented methods for pulse error compensation delineated before, we observed H^u polarisation losses of ca. −5% in bsfb, −10% in H^{C}fb and ufb$_{opt}$, and even −17% in ufb when back-substituting single 180° square pulses for the BIP pairs used. Likewise, up to −25% H^u polarisation was lost by not observing either of the two previously specified rules for optimised relative phase setting.

Table 1 also reveals the effect of progressive saturation of incompletely recovered H^u polarisation when shortening the total interscan delay τ. For instance, recoveries degraded by ca. −40%

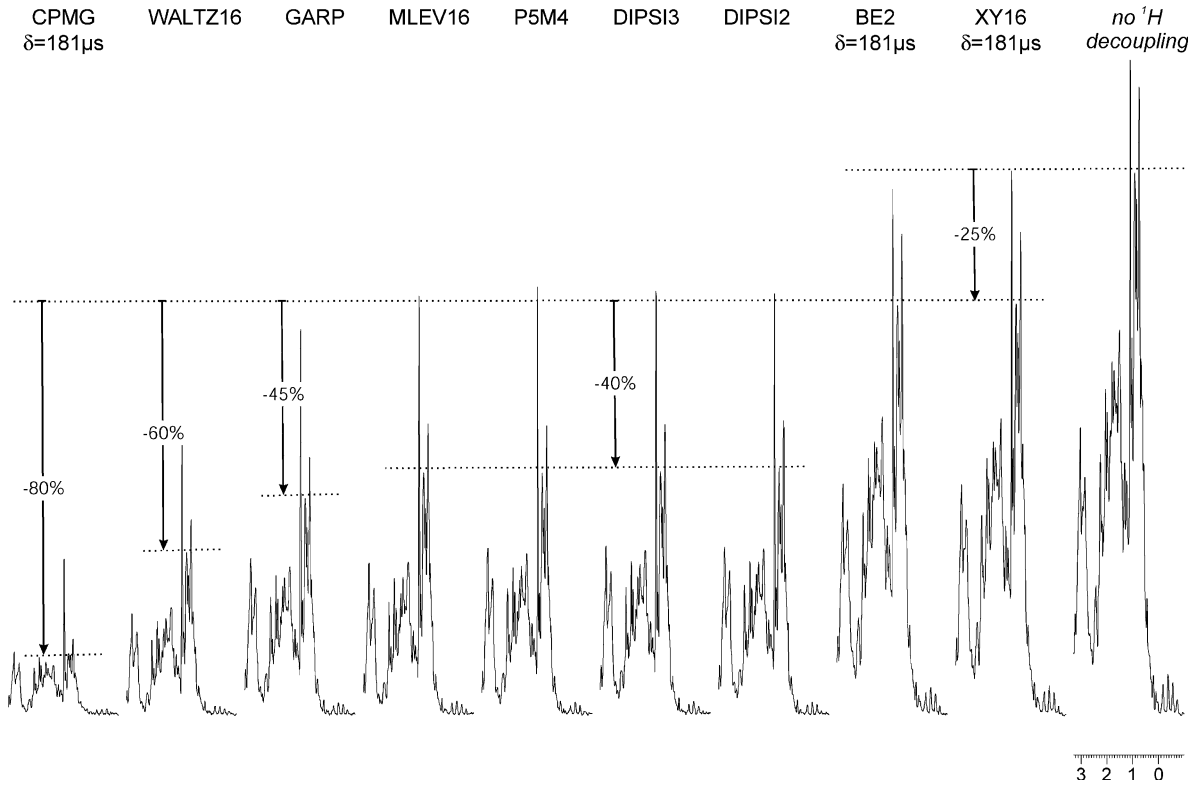

Figure 4. Impact of interim broadband proton decoupling on H^u polarisation recovery. CPMG-derived XY16 (Gullion et al., 1990) and BE2 (Braunschweiler and Ernst, 1983) decoupling best preserve recovered H^u polarisation, causing on average −25% losses relative to ^1H decoupling turned off. All indicated continuous pulsing decoupling sequences degrade H^u magnetisation by ca. 40–60% with respect to XY16 decoupling, mostly due to concomitant T_2 relaxation. Decoupling by classical CPMG, however, largely erodes recovered H^u polarisation due to an inherent lack of compensation for pulse errors. The ^1H spectra (700 MHz, 298 K) were recorded for RTF (153 residues) immediately after an HNCO experiment with bsfb implementation and 2 × 18.4 ms proton decoupling during the $^{15}N \rightarrow {}^{13}CO$ coherence transfer steps, using 181μs echo delays and default high-power 180° square pulses in CPMG-type decoupling.

when reducing τ from 10 to 0.5 s. At $\tau = 10$ s, one may safely assume complete re-equilibration of all ^1H polarisation prior to each scan, and pertaining H^u polarisation recoveries can therefore be equated with the inherent flip-back ratio f_0 afforded by the corresponding efb scheme. Using f_0 and approximate monoexponential $T_1(H^u)$ relaxation times of 1050 ms and 960 ms for CI2 and CHD7, respectively, Equation (7) reproduces the measured $H^u(\tau)$ polarisation recoveries very well (see Table 1).

Figure 4 illustrates the critical impact of interim proton decoupling upon recovered H^u polarisation, which is decisively better preserved by the proposed CPMG-derived decoupling than by any cpd sequence. As discussed before, the latter continuously drives proton magnetisation through the transverse plane, effecting a substantial decay from T_2 relaxation. Contrarily, this attrition factor is virtually eliminated in "windowed" CPMG-type decoupling, where H^u polarisation gets almost instantly inverted at intervals only. The poor tolerance towards offset and imperfections of the constituent inversion pulses, however, almost nullifies H^u polarisation recovery using classical CPMG. Yet, even the simplest 2-step (+/−) phase alternation scheme BE2 (Braunschweiler and Ernst, 1983) largely alleviates this known shortcoming, while more extensive schemes like 16-step XY16 (Gullion et al., 1990) render the inherent error compensation even more robust. Turning proton decoupling off revealed that both XY16 and BE2 decoupling in the given example effect a minimum degradation of H^u polarisation by ca. −25% (due to remaining uncompensated pulse errors and T_1 relaxation, see above). While H^u polarisation was conserved virtually independent

of the CPMG echo delay δ_{CPMG}, chosen between ca. 180 and 620 μs to correspond to full XY16 supercycles, H^N intensities decreased by >5% for $\delta_{CPMG} > 500\mu s$ from increasing admixture of faster antiphase ^{15}N coherence relaxation (data not shown). Relative to optimised XY16 decoupling with $\delta_{CPMG} = 181\mu s$, continuous decoupling using DIPSI2 or 3 (Shaka et al., 1988), MLEV16 (Levitt, 1982) or P5M4 (Tycko and Pines, 1984) degraded H^u polarisation recovery by ca. −40%, while GARP (Shaka et al., 1985) and especially WALTZ16 decoupling (Shaka et al., 1983) fared even worse with −45% and −60% losses, respectively.

Sensitivity enhancements from accelerated H^N relaxation

We next analysed sensitivity enhancements resulting from H^N relaxation acceleration by the recovered H^u polarisation. Using identical parameters as for sampling the H^u polarisation (see above), we recorded the efb-modified HNCO experiments shown in Figure 1 as one-dimensional [NCO]-filtered H^N spectra and varied the number of scans (modulo a minimal phase cycle of 2) while adjusting the total inter scan delay τ such that overall measurement times per 1D spectrum remained constant. Signal-to-noise ratios SN were then derived from bulk integration of all H^N signals.

Figure 5 plots the measured SN^f ratios against τ, proving excellent agreement with the simulated function in the sampled area near τ_{opt} (see close-up insert in Figure 2). Clearly, all presented efb schemes afford the expected shortening of τ^f_{opt} (derived at the maximum SN^f ratio) with respect to the reference water-only flip-back scheme. As listed in Table 2, reductions in τ^f_{opt} and, thus, the effective $T_1{}^f(H^N)$ relaxation time (cf. Equation 2) correlate well with the inherent H^u polarisation recovery f_0 afforded by the efb scheme: up to 35–45% shortening are reached with the most efficient bsfb scheme, followed by ca. 20–30% using ufb_{opt}, ca. 10–20% using ufb and only 5–10% using the least efficient H^Cfb scheme. The corresponding *absolute* sensitivity enhancements SN^f_{max}/SN^0_{max}, however, fall somewhat short of the gains predicted by Equation (8) while still correlating with the extent

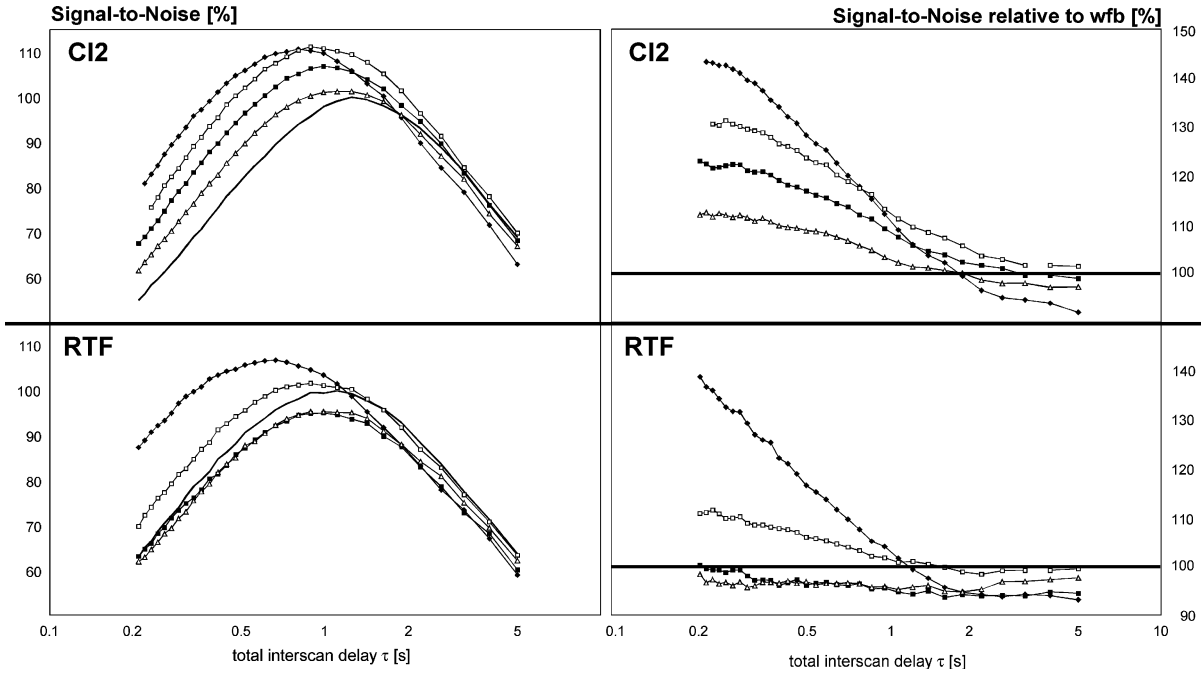

Figure 5. Signal-to-noise ratios from ID H[NCO] employing the different flip-back schemes presented in Figure 1, measured for CI2 (64 residues) and RTF (153 residues): reference wfb (—), bsfb (◆), ufb_{opt} (□), ufb (■) and HCfb (Δ). Plots on the left show signal-to-noise ratios, SN, as percent of the maximum SN_{max} measured with the reference wfb scheme. The corresponding *relative* sensitivity enhancement, calculated as the SN^{efb}/SN^{wfb} ratio between SN values measured at uniform total interscan delay τ using efb and the reference wfb scheme, are shown on the right. Experimental parameters as given for Figure 3.

Table 2. Summarised experimental performance of the efb schemes shown in Figure 1

	HNCO-wfb	HNCO-bsfb	HNCO-ufb$_{opt}$	HNCO-ufb	HNCO-H^{C}fb
RTF (153 residues)					
f_0	0%	52%	32%	27%	21%
c^f	≡ 1.00	0.94	1.00	0.94	0.98
τ_{opt} [ms]	1100	660 (−40%)	880 (−20%)	975 (−11%)	1050 (−5%)
SN^f_{max}/SN^0_{max}	≡ 1.00	1.08 {1.}	1.02 {2.}	0.95 {−}	0.95 {−}
$[SN^f/SN^0]_{max}$	≡ 1.00	1.55 {1.}	1.20 {2.}	1.03 {3.}	1.03 {3.}
CHD7 (80 residues)					
f_0	0%	62%	52%	47%	33%
c^f	≡ 1.00	0.92	0.98	0.97	0.95
τ_{opt}[ms]	1100	625 (−43%)	800 (−27%)	880 (−20%)	1000 (−9%)
SN^f_{max}/SN^0_{max}	≡ 1.00	1.11{1.}	1.05 {2.}	1.01 {3.}	0.95 {−}
$[SN^f/SN^0]_{max}$	≡ 1.00	1.70{1.}	1.20{2.}	1.20{2.}	1.05 {3.}
CI2 (64 residues)					
f_0	0%	63%	56%	50%	30%
c^f	≡ 1.00	0.93	1.01	0.99	0.97
τ_{opt} [ms]	1225	800 (−35%)	900 (−26%)	1000 (−18%)	1150 (−6%)
SN^f_{max}/SN^0_{max}	≡ 1.00	1.11 {2.}	1.12 {1.}	1.07 {3.}	1.01 {4.}
$[SN^f/SN^0]_{max}$	≡ 1.00	1.40 {1.}	1.35 {2.}	1.20 {3.}	1.10 {4.}

SN^f_{max}/SN^0_{max} (with $SN^0_{max} = SN^{wfb}_{max}$) is the *absolute* sensitivity enhancement relevant for measurements limited by sensitivity requirements when using the pertaining optimised interscan delays τ_{opt} (i.e., *optimal pulsing regime*). $[SN^f/SN^0]_{max}$ (extrapolated using Equation 6) is the predicted maximal *relative* sensitivity enhancement relevant for measurements limited by resolution requirements when using identical interscan delays shorter than τ_{opt} (i.e., *fast pulsing regime*). Sensitivity enhancements with respect to the reference wfb experiment have been ranked (in curly brackets), with "–" indicating an actual sensitivity decrease due to additional relaxation losses on the H^N coherence path. f_0 = intrinsic H^u flip-back ratio (measured for $\tau = 10$s, see Table 1), $c^f = H^N$ scaling factor (extrapolated from SN^f/SN^0 for $\tau \gg \tau_{opt}$ with $c^f = c^0 = 1$ for wfb), τ_{opt} = optimal total interscan delay (with shortening relative to wfb given in brackets). All measured data (at 700 MHz, 298 K) was determined from corresponding bulk integrals of the 1D ^{1}H[HNCO] spectra; experimental parameters as given for Table 1.

of H^u polarisation recovery for each separate efb scheme. They range between only 2% for the large RTF and 12% for the small CI2 protein using the T_2 relaxation-affected ufb$_{opt}$ scheme, while ca. 10% are gained for all tested proteins with the largely T_2-insensitive bsfb scheme. In contrast, both ufb and H^{C}fb schemes may actually degrade the H^N signal-to-noise ratio particularly for larger proteins. These discrepancies, along with the apparent divergence of the measured SN at long $\tau \gg \tau^f_{opt}$ are largely due to inherent H^N intensity losses for the different efb schemes that reduce their pertaining scaling factors c^f (cf. Equations 4–6) below 1. The latter may be extrapolated for long τ from the plot of *relative* sensitivity enhancements, $[SN^f/SN^0]$, shown in Figure 5 (cf. Equation 5). There, SN^f ratios eventually drop below SN^0 except for the ufb$_{opt}$ and, only for the small CI2 protein, the ufb schemes. With bsfb, ca. 6–8% losses in bulk H^N intensity accumulated for both the small CI2 and the large RTF proteins, indicating that they have causes other than size-dependent relaxation. These apparent losses are in fact provoked by imperfectly band-selective flip-back pulses that partially degrade the low-frequency H^N signals included in the evaluated bulk integrals. Contrarily, H^N intensity losses inherent in the ufb scheme amount to −6% for the large RTF, but have largely vanished for the smaller CI2 and CHD7 proteins. This size-dependence indicates some additional relaxation during the coherence path in ufb as origin for the losses, i.e. the predicted additional $R_1(2N_zH_z)$ relaxation during the inserted H^u rephasing delay Δ'. Finally, while SN^{HCfb} measured with the H^{C}fb scheme for CI2 diverges from SN^{wfb} at long τ by ca. −3%, due mostly to additional $R_1(2N_zCO_z)$ relaxation on the coherence path (see above), the ratios appear to eventually converge for RTF. Here, however, ca. −5% H^N intensity losses accrue at intermediate τ, putatively reflecting the effect of

inferior water flip-back in the H^Cfb scheme (see above). *Relative* sensitivity enhancements $[SN^f/SN^0](\tau)$ increased monotonously up to the shortest sampled $\tau = 200$ ms, where ratios reached ca. 40–45% for all three test proteins using the most efficient bsfb scheme (Figure 5, CHD7 data not shown). With both c^f and τ^f_{opt} determined from the experimental SN data, we employed Equation (6) to extrapolate maximal *relative* SN enhancements, $[SN^f/SN^0]_{max}$, at shorter interscan delays (see Table 2). Unfortunately, we were not able to experimentally access this extremely fast pulsing regime on our BRUKER DRX700 spectrometer due to recurring hardware failure for τ<200 ms. Nevertheless, the predicted $[SN^f/SN^0]_{max}$ ratios agree strikingly well with the maxima emerging from the experimental data for CI2 (Figure 5b), i.e. ca. 140–145% with bsfb, up to 130% with ufb_{opt}, around 120–125% with ufb and still ca. 110–115% with H^Cfb. For RTF, no clear leveling-off is observed for the $[SN^f/SN^0]_{max}$ ratios up to the shortest sampled $\tau \approx 200$ ms; the predicted $[SN^f/SN^0]$ ratios of up to 155% with bsfb, 120% with ufb_{opt}, but only ca. 103% with ufb and H^Cfb appear, however, well within reach (similar observations hold for CHD7).

The good agreement of sampled $[SN^f/SN^0]$ ratios with the maximal $[SN^f/SN^0]_{max}$ extrapolated using Equation (6) is somewhat surprising, considering that H^u polarisation recovery decreases along with τ due to saturation (cf. Equation 7). The expected decrease of $[SN^f/SN^0]$ ratios in the very fast pulsing regime may therefore only occur for $\tau < 200$ ms, and the approximate experimental maxima do not appear to fall far below the $[SN^f/SN^0]_{max}$ enhancements calculated assuming constant $R_1^f(H^N)$ relaxation rates. A clear correlation between H^u polarisation recovery and the afforded acceleration of H^N relaxation is nevertheless obvious from Figure 6 that plots acceleration ratios $R_1^f(H^N)/R_1^0(H^N) = \tau^0_{opt}/\tau^f_{opt}$ (cf. Equation 2) against the intrinsic H^u flip-back ratios f_0 afforded by the presented efb schemes. It is reasonable to assume that the observed increase in acceleration ratios with increasing f follows a sigmoidal curve up to a characteristic maximum. The data furthermore shows that acceleration rates increase with the protein size, corroborating the well-known fact that the underlying dipolar coupling between H^N and H^u polarisations (''spin diffusion'') is more substantial for larger proteins.

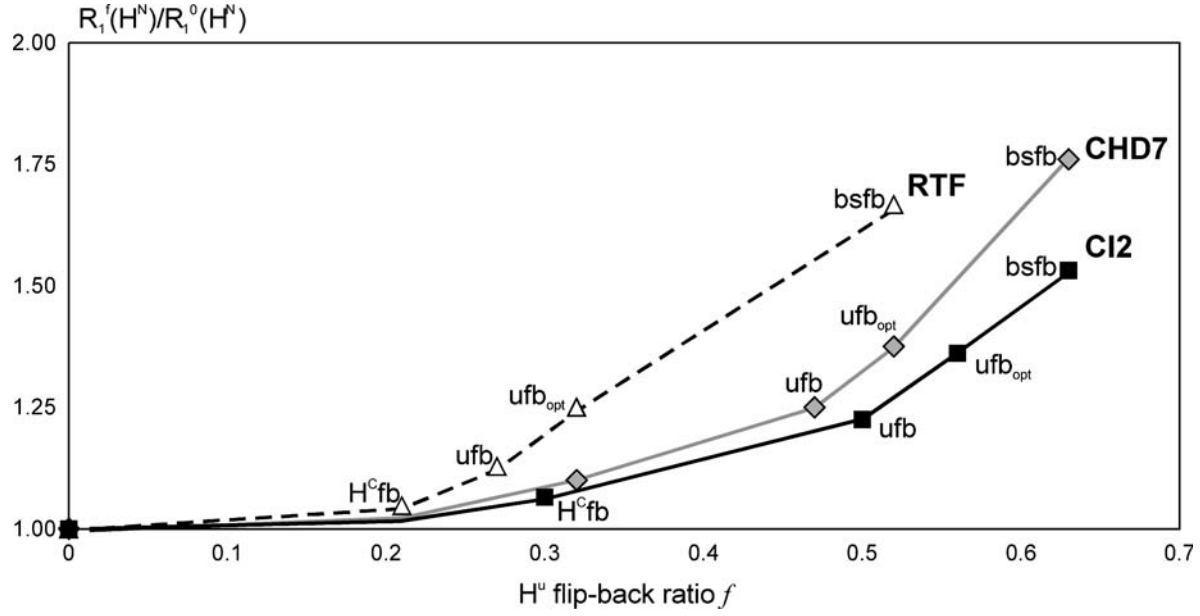

Figure 6. Acceleration ratios for longitudinal H^N relaxation (relative to wfb implementation) versus H^u polarisation recovery for CI2 (■, 64 residues), CHD7 (◆, 80 residues) and RTF (Δ, 153 residues). Data was taken from Table 2 for the indicated efb schemes and $\tau = 10$ s (i.e. depicted f correspond to f_0). Acceleration ratios $R_1^f(H^N)/R_1^0(H^N)$ were calculated from the experimentally determined optimal interscan delays τ_{opt} using Equation (2). Experimental parameters as given for Table 1.

Thus, H^u polarisation recovery as a method for sensitivity or resolution enhancement would become ever more powerful for proteins with increasing size and proton density. The efficiency of flip-back schemes, however, decreases in the same order due to some inevitable H^u magnetisation decay from transverse $T_2(H^u)$ relaxation. Consequently, maximal sensitivity gains by efb should be reached for proteins with intermediate size. In our tests at 700 MHz and 298 K, using the basic HNCO experiment with the most efficient bsfb scheme, CHD7 with its intermediate size of 80 residues benefitted the most (see Figure 6). As discussed, bsfb accrues only minimal T_2 relaxation losses for the recovered H^u polarisation, making it the single most efficient efb scheme for larger proteins. For smaller proteins, universal flip-back schemes passively exploiting the $^1J_{HN}$ coupling become increasingly competitive, especially the presented ufb_{opt} scheme that may, however, only be used for HNCO-type experiments. The H^Cfb scheme, actively exploiting the non-uniform $^1J_{HC}$ coupling, affords by far the lowest H^u polarisation recovery and, offering no particular advantages, may probably be discarded.

Conclusion

We have presented several extended flip-back schemes (efb) to recover unselected H^u proton polarisation in multidimensional HSQC-type out-and-back experiments with the object of enhancing intensities by accelerating H^N re-equilibration. The performance of these efb schemes was tested using the basic HNCX experiment (CX = CO or CA) and several test proteins of different size. The proposed band-selective flip-back scheme (bsfb) generally affords the highest H^u polarisation recovery, showing the smallest degradation by $T_2(H^u)$ relaxation, yet at the price of possible intensity losses for low-frequency H^N signals. The novel schemes for universal flip-back (ufb and ufb_{opt}) do not suffer from this complication, but are substantially more susceptible to T_2 relaxation losses degrading H^u polarisation recovery. They therefore become competitive mostly for smaller proteins. Contrarily, polarisation recovery in the H^Cfb scheme appears too inefficient to override intrinsic additional relaxation losses on the H^N coherence transfer path. These also accrue in the simple ufb scheme, but not in ufb_{opt} that may, however, only be used for CX = CO. In all schemes, crucial improvements in preserving recovered H^u polarisation were afforded by the novel use of CPMG-derived sequences for the required interim proton decoupling, and by implementing broad-band inversion pulses.

With intrinsic H^u polarisation recoveries reaching up to 60%, we observed substantial sensitivity enhancements with respect to the conventional water-only flip-back scheme (wfb) from accelerated H^N re-equilibration. These gains increase with the pulsing rate and reached ca. 40% at the shortest sampled total interscan delay $\tau = 200$ ms for all tested proteins, using the most efficient bsfb scheme. An expression to assess the maximal sensitivity enhancement achievable was derived, well reproducing the experimental data and predicting gains of up to 70% at even shorter τ. Yet, enhancements are expected to eventually drop again due to increasing saturation of recovered H^u polarisation, for which an equation was likewise derived. Acceleration of H^N re-equilibration and pertaining sensitivity enhancement as expected also increased with the extent of H^u polarisation recovery and spin diffusion (i.e. the strength of dipolar interaction between H^N and H^u polarisations). While the latter effect increases with protein size and proton density, the former decreases from more $T_2(H^u)$ relaxation losses inevitably accumulating in the efb scheme. Sensitivity enhancement by efb should therefore reach a maximum for proteins of intermediate size (ca. 100 residues).

In conclusion, sensitivity enhancements from efb are particularly pronounced when measurement times are dictated by resolution requirements and interscan re-equilibration delays τ shorter than the optimal $\tau^f_{opt} = 1.25 \cdot T_1(H^N)$ are used (*fast pulsing regime*). Conversely, in the sensitivity-limited measurement regime, the longer pertaining τ^f_{opt} delay should be employed (*optimal pulsing regime*), and absolute sensitivity enhancements then afforded by efb are less significant. Again, bsfb affords the greatest sensitivity enhancement, followed by ufb_{opt} (applicable only to HNCO-derived experiments) and, for small proteins only, the simple ufb scheme, while H^Cfb is too inefficient or even detrimental.

Acknowledgements

The generous supply of doubly labelled CHD7, USP and RTF test proteins by Mark Daniels, Rob de Jong and Gert Folkers, and of CI2 by Rolf Boelens, is gratefully acknowledged. T.D. thanks Vladislav Orekhov for stimulating discussions. This work was financially supported by the EU Structural Proteomics in Europe (SPINE) contract (QLG2-CT-2002-00988).

Appendix

Saturation decay of steady-state polarisation recovery

An equation to calculate steady-state H^u polarisation recovery under conditions of progressive saturation (i.e., for short interscan re-equilibration delays τ) may be directly adapted from a related equation describing longitudinal interference in repetitive pulse experiments (Ernst et al., 1987), or independently derived *ab initio* as follows:

Starting with fully re-equilibrated proton polarisation, ${H_0}^u$, a fraction f_0 (i.e., the intrinsic flip-back ratio afforded by a given efb scheme) is recovered by the end of the first scan. During the subsequent interscan delay τ, longitudinal $R_1(H^u)$ relaxation partially replenishes H^u polarisation that now deviates by a fraction $[1-f]$ from equilibrium. The polarisation at the start of the second scan will then be:

$$H^u(2)^{\text{start}} = H_0^u \cdot [1 - [1 - f_0] \cdot \exp(-\tau \cdot R_1(H^u))]$$

Introducing x as short notation for the exponential relaxation factor and the fractional H^u polarisation at the start of scan n, $f(n)^{\text{start}} = H^u(n)^{\text{start}}/{H^u}_0$ we can simplify to:

$$f(2)^{\text{start}} = [1 - [1 - f_0] \cdot x] = (1 - x) + f_0 \cdot x$$

By the end of scan 2, again only a fraction f_0 is recovered. H^u polarisation, now deviating by $[1 - f_0 \cdot f(2)^{\text{start}}]$ from equilibrium, once more partially relaxes during the subsequent interscan delay τ_{inter} to yield the fractional start polarisation for scan 3:

$$\begin{aligned} f(3)^{\text{start}} &= 1 - [1 - f_0 \cdot f(2)^{\text{start}}] \cdot x \\ &= (1 - x) + f_0 \cdot x \cdot f(2)^{\text{start}} \end{aligned}$$

Substituting the previous expression for $f(2)^{\text{start}}$ yields:

$$\begin{aligned} f(3)^{\text{start}} &= (1 - x) + f_0 \cdot x \cdot [(1 - x) + f_0 \cdot x] \\ &= (1 - x) \cdot [1 + f_0 \cdot x] + f_0^2 \cdot x^2 \end{aligned}$$

Again, a fraction f_0 is recovered and, deviating by $[1 - f_0 \cdot f(3)^{\text{start}}]$ from equilibrium, partially relaxes during the next delay τ_{inter} to produce the starting polarisation for scan 4:

$$\begin{aligned} f(4)^{\text{start}} &= 1 - [1 - f_0 \cdot f(3)^{\text{start}}] \cdot x = (1 - x) \\ &\quad + f_0 \cdot x \cdot [(1 - x) \cdot [1 + f_0 \cdot x] + f_0^2 \cdot x^2] \end{aligned}$$

This expression simplifies to:

$$f(4)^{\text{start}} = (1 - x) \cdot \left[1 + f_0 \cdot x + f_0^2 \cdot x^2\right] + f_0^3 \cdot x^3$$

Clearly,a geometrical series emerges for calculating the starting polarisation at later scans n:

$$\begin{aligned} f(n)^{\text{start}} &= (1 - x) \cdot \left[\sum_{i=1}^{n-1} (f_0 x)^{i-1}\right] + (f_0 x)^{n-1} \\ &= (1 - x) \cdot \frac{1 - (f_0 x)^{n-1}}{1 - f_0 x} + (f_0 x)^{n-1} \end{aligned}$$

With increasing number of scans, this expression rapidly converges since $f_0 \cdot x$ invariably is < 1, i.e. $(f_0 x)^{n-1}$ approaches zero. The limiting value, multiplied by the fraction f_0 regained *after* the scan and now only depending on the experimental interscan delay, τ, is the desired fractional steady-state H^u polarisation recovered:

$$\begin{aligned} f(\tau) &= f_0 \cdot \lim_{n \to \infty} f(n)^{\text{start}} = f_0 \cdot \frac{1 - x}{1 - fx} \\ &= f_0 \cdot \frac{1 - \exp(-\tau \cdot R_1(H^u))}{1 - f_0 \cdot \exp(-\tau \cdot R_1(H^u))} \end{aligned}$$

References

Abragam, A. (1961) In *Principles of Nuclear Magnetism. The International Series of Monographs on Physics* Adair, R.K., Elliott, R.J., Marshall, W.C. and Wilkinson, D.H. (Eds.), Clarendon Press, Oxford/UK.

Braunschweiler, L. and Ernst, R.R. (1983) *J. Magn. Reson.*, **53**, 521–528.
Emsley, L. and Bodenhausen, G. (1992) *J. Magn. Reson.*, **97**, 135–148.
Ernst, R.R., Bodenhausen, G. and Wokaun, A. (1987) In *Principles of Nuclear Magnetic Resonance in One and Two Dimensions. The International Series of Monographs on Chemistry* Rowlinson, J.S. (Ed.), 14, Clarendon Press, Oxford/UK.
Furrer, J., Kramer, F., Marino, J.P., Glaser, S.J. and Luy, B. (2004) *J. Magn. Reson.*, **166**, 39–46.
Geen, H. and Freeman, R. (1991) *J. Magn. Reson.*, **93**, 93–141.
Gullion, T., Baker, D. and Conradi, M.S. (1990) *J. Magn. Reson.*, **89**, 479–484.
Hallenga, K. and Lippens, G.M. (1995) *J. Biomol. NMR*, **5**, 59–66.
Hiller, S., Wider, G., Etezady-Esfarjani, T., Horst, R. and Wüthrich, K. (2005) *J. Biomol. NMR*, **32**, 61–70.
Kay, L.E., Xu, G.Y. and Yamazaki, T. (1994) *J. Magn. Reson.*, **A109**, 129–133.
Levitt, M.H. (1982) *J. Magn. Reson.*, **48**, 234–264.
Ludvigsen, S., Shen, H., Kjaer, M., Madsen, J.C. and Poulsen, F.M. (1991) *J. Mol. Biol.*, **222**, 621–635.
Meiboom, S. and Gill, D. (1958) *Rev. Sci. Instrum.*, **29**, 688–691.
Pervushin, K., Vögeli, B. and Eletsky, A. (2002) *J. Am. Chem. Soc.*, **124**, 12898–12902.
Riek, R., Fiaux, J., Bertelsen, E.B., Horwich, A.L. and Wüthrich, K. (2002) *J. Am. Chem. Soc.*, **124**, 12144–12153.
Sattler, M., Schleucher, J. and Griesinger, C. (1999) *Progr. NMR Spectr.*, **34**, 93–158.
Schanda, P. and Brutscher, B. (2005) *J. Am. Chem. Soc.*, **127**, 8014–8015.
Shaka, A.J., Barker, P.B. and Freeman, R. (1985) *J. Magn. Reson.*, **64**, 547–552.
Shaka, A.J., Keeler, J., Frenkiel, T. and Freeman, R. (1983) *J. Magn. Reson.*, **52**, 335–338.
Shaka, A.J., Lee, C.J. and Pines, A. (1988) *J. Magn. Reson.*, **77**, 274–293.
Skinner, T.E., Reiss, T.O., Luy, B., Khaneja, N. and Glaser, S.J. (2004) *J. Magn. Reson.*, **167**, 68–74.
Sklenar, V. (1995) *J. Magn. Reson.*, **A114**, 132–135.
Sklenar, V., Piotto, M., Leppik, R. and Saudek, V. (1993) *J. Magn. Reson.*, **A102**, 241–245.
Smith, M., Hu, H. and Shaka, A.J. (2001) *J. Magn. Reson.*, **151**, 269–283.
Tycko, R. and Pines, A. (1984) *Chem. Phys. Lett.*, **111**, 462–467.
Zweckstetter, M. and Holak, T.A. (1999) *J. Biomol. NMR*, **15**, 331–334.